ELSEVIER

Chemical Physics 204 (1996) 469–478

Chemical Physics

The electronic structures and magnetic properties of one-dimensional ABO_6 chains in Sr_3ABO_6 (A = Co, Ni; B = Pt, Ir) and two-dimensional MO_3 sheets in $InMO_3$ (M = Fe, Mn) [1]

Grigori V. Vajenine [a], Roald Hoffmann [a], Hans-Conrad zur Loye [b]

[a] *Department of Chemistry, Cornell University, Ithaca, NY 14853-1301, USA*

[b] *Department of Chemistry, Massachusetts Institute of Technology, 77 Massachusetts Avenue, Cambridge, MA 02139, USA*

Received 15 January 1995

Abstract

Extended Hückel calculations were carried out on the electronic structure of one-dimensional ABO_6 chains in Sr_3ABO_6 (A = Co, Ni; B = Pt, Ir) and two-dimensional MO_3 sheets in $InMnO_3$ (M = Fe, Mn). The band structures were compared to the levels of model fragments in an attempt to understand the nature of metal-metal interactions in these oxides. In the ABO_6 chains it appears that both direct and oxygen-mediated A–B interactions are very small. In the MO_3 sheets only an indirect M–O–M intralayer interaction was found to be significant. The relationship between the band structures and the magnetic properties of the oxides is discussed.

1. Introduction

Recently, representatives of two groups of low-dimensional oxides with interesting magnetic properties were synthesized. The first group contains oxides of the formula Sr_3ABO_6 (A = Co, Ni; B = Pt, Ir) [1]. These structures contain parallel one-dimensional ABO_6^{6-} chains well-separated by Sr^{2+} ions. Each metal atom of type B is surrounded by six O atoms forming a trigonal antiprism. A distorted trigonal prism of O atoms is found around each metal atom of type A. The chains are formed by alternating AO_6 and BO_6 polyhedra sharing faces, along what we will denote as the z axis, **1**.

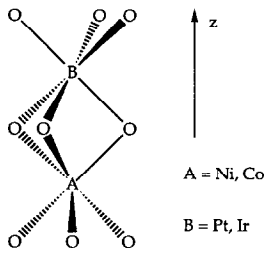

1

The other group includes oxides of the stoichiometry $InMO_3$ (M = Fe, Mn) [2]. These are comprised of MO_3^{3-} layers separated by In^{3+} ions, each indium ion surrounded by a trigonal antiprism of oxygens. Each M^{3+} ion has five oxygens around it forming a trigonal bipyramid (the MO_3^{3-} layers lie in the xy-plane, the axial oxygens are shown only for the central M atom), **2**.

[1] Dedicated to Bernard Pullman on the occasion of his 75th birthday.

0301-0104/96/$15.00 © 1996 Elsevier Science B.V. All rights reserved
SSDI 0301-0104(95)00335-5

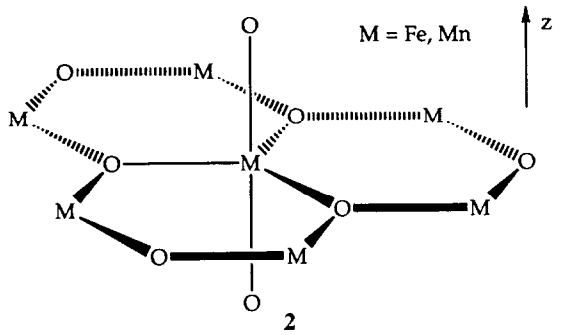

2

As in the previous group of compounds, it seems that the In^{3+} ions merely separate the MO_3^{3+} layers, without significantly affecting intralayer interactions. This allows us again to focus on a substructure of lower dimensionality than that of the three-dimensional oxides themselves.

2. Calculations

Band structure calculations, as well as molecular calculations on model compounds were carried out for both groups of compounds. We used the extended Hückel method [3] with the atomic parameters given in Table 1. The geometries studied were those experimentally obtained for the corresponding crystals [1,2]. When a calculation on a substructure (e.g. an ABO_6 chain, a MO_3 sheet, an AO_6, BO_6, or MO_5 fragment) was performed, the geometry of the substructure was taken to be the same as it was in the crystal.

2.1. Sr_3ABO_6

First, we consider the band structure of a one-dimensional $NiPtO_6^{6-}$ chain present in Sr_3NiPtO_6, a representative of the first group of oxides. It is useful to begin by looking at the electronic structure of the component PtO_6 and NiO_6 building blocks of the chain. The metal–oxygen distances are 2.04 Å in the former and 2.17 Å in the latter. Since the geometry of the PtO_6 fragment is nearly octahedral, the Pt metal d-orbitals should form a typical 'three below two' splitting pattern. For the approximately trigonal prismatic NiO_6 center one would also expect a three below two pattern, the ordering of the lower three levels depending on the detailed geometry of the complex. The energies of the molecular orbitals in question are shown below in **3**. The C_3 axis in each fragment is aligned with the z-axis.

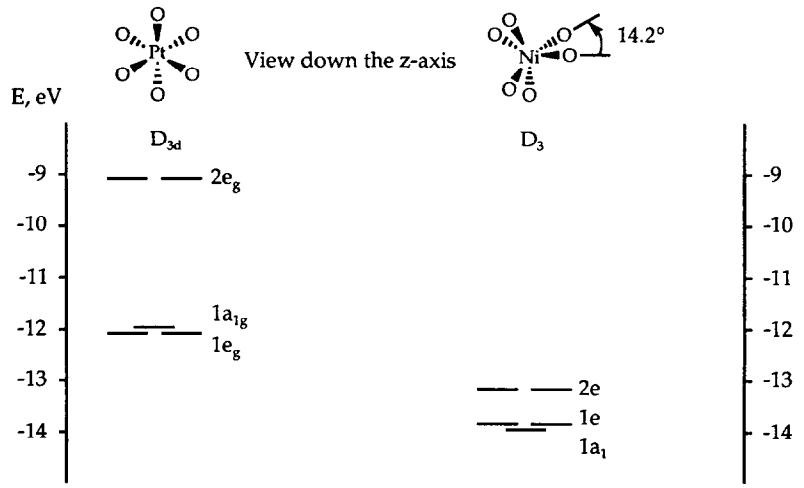

3

Table 1
Atomic parameters used in extended Hückel calculations

Atom	Orbital	H_{ii} (eV)	ζ_1	c_1	ζ_2	c_2
O	2s	−32.3	2.275			
	2p	−14.8	2.275			
Sr	5s	−6.62	1.214			
	5p	−3.92	1.214			
Co	4s	−9.21	2.0			
	4p	−5.29	2.0			
	3d	−13.18	5.55	0.5680	2.10	0.6060
Ni	4s	−10.95	2.10			
	4p	−6.27	2.10			
	3d	−14.2	5.75	0.5683	2.30	0.6292
Pt	6s	−9.077	2.554			
	6p	−5.475	2.554			
	5d	−12.59	6.013	0.6334	2.696	0.5513
Ir	6s	−11.36	2.50			
	6p	−4.50	2.20			
	5d	−12.17	5.796	0.6698	2.557	0.5860
In	5s	−12.60	1.903			
	5p	−6.19	1.677			
Fe	4s	−9.10	1.9			
	4p	−5.32	1.9			
	3d	−12.6	5.35	0.5505	2.00	0.6260
Mn	4s	−9.75	1.8			
	4p	−5.89	1.8			
	3d	−11.67	5.15	0.5320	1.90	0.6929

Indeed, one finds the expected level ordering; the strength of the crystal field is greater for Pt. Drawings of the orbitals [4] may be found in Fig. 1. The magnitudes of the level splitting [2] computed are consistent with those found in isolated octahedral complexes of Ni^{2+} and Pt^{4+}.

We next examined the one-dimensional $NiPtO_6^{6-}$ chain. The resulting band structure, density of states [7] (DOS), as well as contributions of Pt and Ni d-orbitals to the DOS are shown in Fig. 2. The metal d-orbitals remain at the same energy as in the isolated model complexes. The d-bands are very narrow – the DOS plot exaggerates the actual band width because each band is effectively broadened in the computation. The narrow metal bands suggest a lack of direct, or for that matter, oxygen-bridge-mediated Pt-Ni interaction. The band structures of the similar $CoPtO_6^{6-}$ and $NiIrO_6^{6-}$ chains are qualitatively the same, the only difference being in the energies of the d-orbitals (see Figs. 3, 4). The crystal orbital overlap population [7] (COOP) analysis (not shown in graphical detail here) also indicates no Pt–Ni, Co–Pt, and Ni–Ir bonding. The computed values of the OP are −0.0077 for Ni–Pt, −0.0119 for Co–Pt, −0.0183 for Ni–Ir.

The DOS for an isolated $NiPtO_6^{6-}$ chain is virtually identical to the DOS for the same chain in the three-dimensional solid Sr_3NiPtO_6 solid, also computed by us (but not shown here). There is only about 3% of Sr states in the energy window of Fig. 2. That confirms the absence of interchain interactions.

To summarize, the calculations indicate that metal atoms A and B interact weakly within their one-dimensional chains, which is not surprising given the A–B distance of 2.8 Å. All compounds considered above were found experimentally to be insulating [1], although they contain metal atoms with unpaired electrons. This is consistent with the small dispersion of the metal d-bands obtained in our calculations. The magnetic properties depend strongly on the number of unpaired electrons on the metal atoms comprising the one-dimensional chains [1].

Magnetic susceptibility studies of polycrystalline Sr_3NiPtO_6 indicate the onset of antiferromagnetic ordering at ~ 25 K (Fig. 5). The susceptibility data does not show the typical cusp of an antiferromagnet, but rather flattens out, which is often observed in low-dimensional materials. A fit to the magnetic data indicates that the nickel atoms are able to couple weakly antiferromagnetically at low temperatures, as indicated by the leveling of the susceptibility; the magnetic exchange is only short range in nature, which is not surprising considering the nickel-nickel distance of 5.6 Å. Thus, although Sr_3NiPtO_6 is structurally a chain, its magnetic properties are best described as those of isolated, very weakly coupled, nickel(II) atoms.

The extended Hückel calculations indicate the absence of any bonding interactions between the nickel and the neighboring platinum atoms (Ni–Pt distance = 2.8 Å). The antiferromagnetic coupling between the nickel atoms, presumably through a superexchange pathway involving the diamagnetic platinum, are weak and insufficient to establish long range magnetic order.

[2] The crystal field splitting found in $Ni(H_2O)_6^{2+}$ is 1.1 eV [5]. The splitting in $PtCl_6^{2-}$ and $PtBr_6^{2-}$ are 3.9 and 3.1 eV, respectively, estimated from spectroscopic data in Ref. [6].

In contrast, Sr_3NiIrO_6, a structural, but not a magnetic, analog of Sr_3NiPtO_6, undergoes long range magnetic ordering [8]. Substitution of diamagnetic, low-spin octahedral platinum (IV), by low-spin octahedral iridium (IV), (d^5), places an element having one unpaired electron into the octahedral site. Thus, instead of having alternating paramagnetic and diamagnetic centers, as in the platinum oxide, the iridium compound has an octahedral site with one unpaired electron alternating with trigonal prismatic sites containing nickel with two unpaired electrons. The additional interactions between the electrons on the trigonal prismatic site and the single unpaired electron on the octahedral site lead to the more complex magnetic behavior shown in Fig. 6.

Although there is no evidence of nickel–iridium

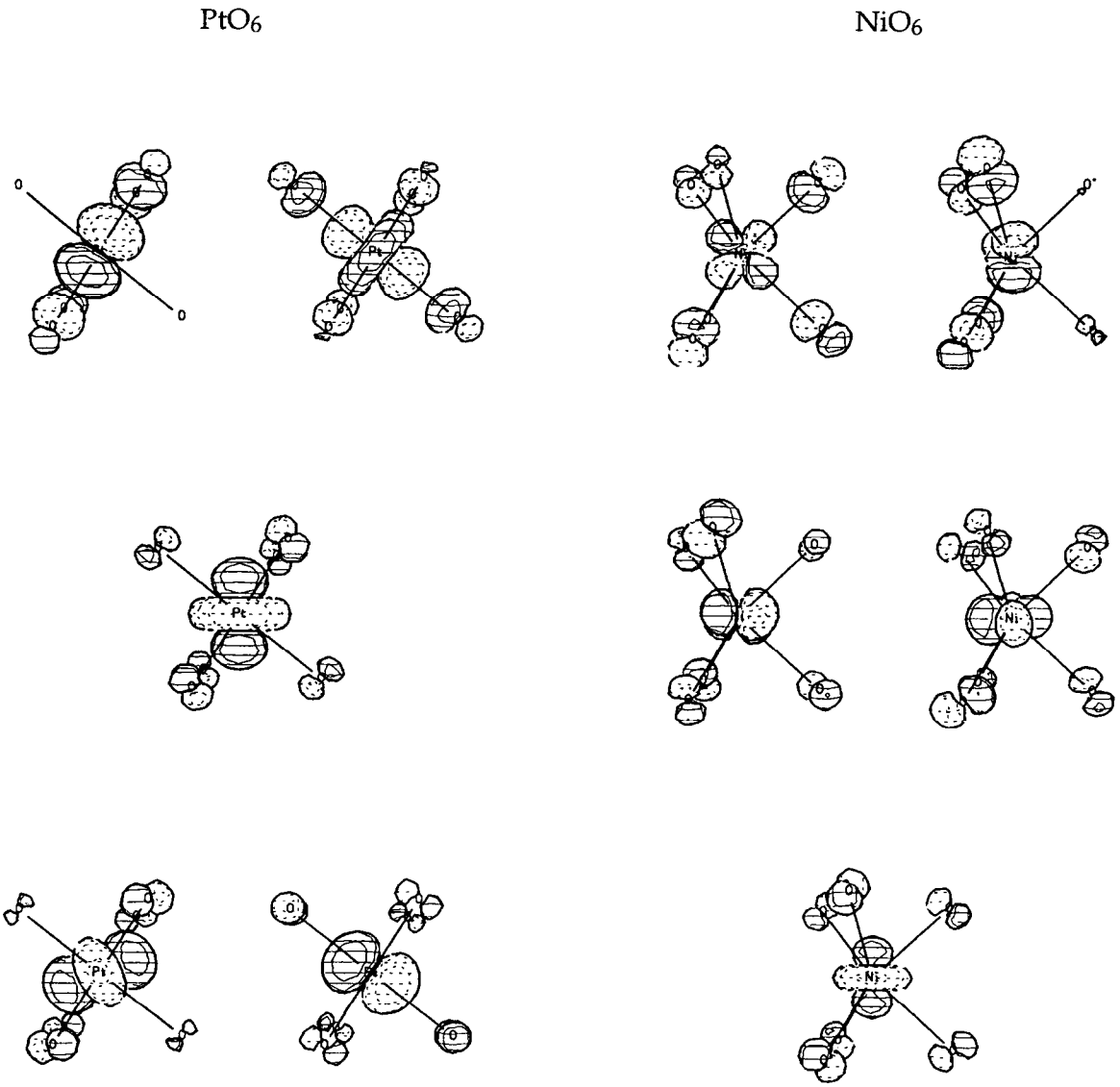

Fig. 1. Drawing of molecular orbitals with mainly metal d-character in PtO_6 and NiO_6 fragments. The view is from the side, perpendicular to the z-axis.

bonding by extended Hückel calculations, the presence of the unpaired electron on the iridium creates stronger magnetic coupling than was observed for Sr_3NiPtO_6. The metal atoms along the chains are ferromagnetically correlated, as indicated by a positive deviation from Curie-like behavior noticeable below 150 K and, more strongly, below 70 K, until ~ 21 K, when there is a sharp transition to a singlet ground state. Clearly there exist magnetic interactions between the nickel and the iridium (Ni–Ir distance = 2.8 Å), which however do not show up in the extended Hückel calculations.

An intermediate case is provided by Sr_3CoPtO_6. Magnetic studies of polycrystalline Sr_3CoPtO_6 indicate Curie-like paramagnetism, as shown in Fig. 7. A fit of the data to the Curie–Weiss law reveals two unusual features: a small Weiss constant, $\theta = 3.12$ K, and an unexpected moment of 5.96 μ_B. Five unpaired electrons would be expected to give a spin-only moment of 5.92 μ_B. Clearly, this system does not contain Pt(IV) and Co(II), since this combination of oxidation states would give at most three unpaired electrons – three electrons from cobalt and zero electrons from low-spin platinum. One combination of oxidation states that could account for five unpaired electrons, as well as maintain charge balance, includes Co(III) and a mixture of Pt(II)/Pt(IV). High-spin, d^6 Co(III) in trigonal prismatic coordination would contribute four unpaired electrons. If platinum in the octahedral site disproportionates into Pt(II), d^8, and Pt(IV), d^6, then, on average, the platinum would contribute one unpaired electron. The existence of both Pt(II) and Pt(IV) was confirmed by XPS studies. Interestingly, there exists no ordering of Pt(II) and Pt(IV) along the chain; that is, Pt(II) and Pt(IV) randomly occupy the single octahedral site in the chain structure.

This compound represents an intermediate case between Sr_3NiPtO_6 and Sr_3NiIrO_6 in that sometimes the nickel has a nearest neighbor platinum atom containing no unpaired electrons, similar to Sr_3NiPtO_6, and sometimes the nickel has a nearest neighbor platinum containing two unpaired electrons, similar to in Sr_3NiIrO_6. Consequently, we can envi-

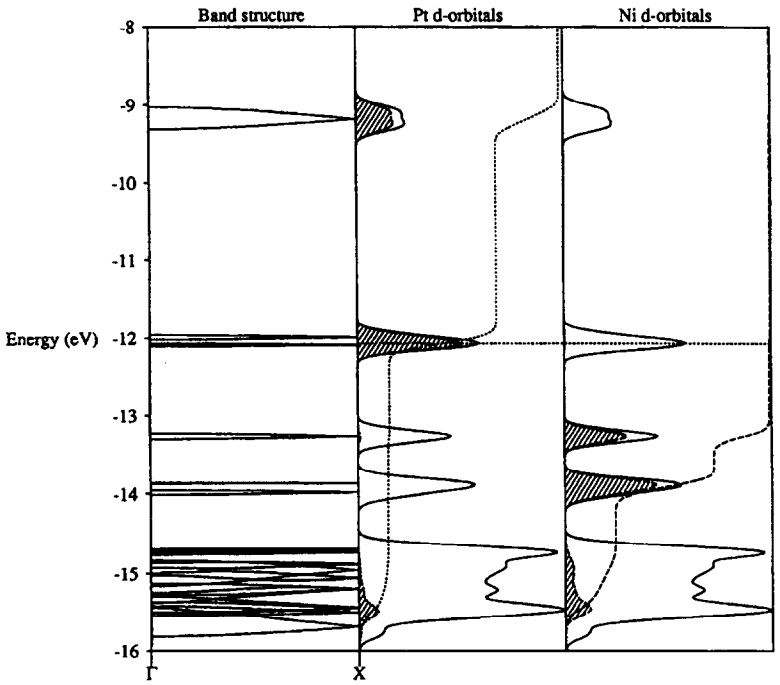

Fig. 2. From left to right: band structure for a $NiPtO_6^{6-}$ chain; total DOS (solid line), projection of Pt d-orbitals (lined), integration of the projection (dotted line); total DOS (solid line), projection of Ni d-orbitals (lined), integration of the projection (broken line). The horizontal dotted line indicates the Fermi level.

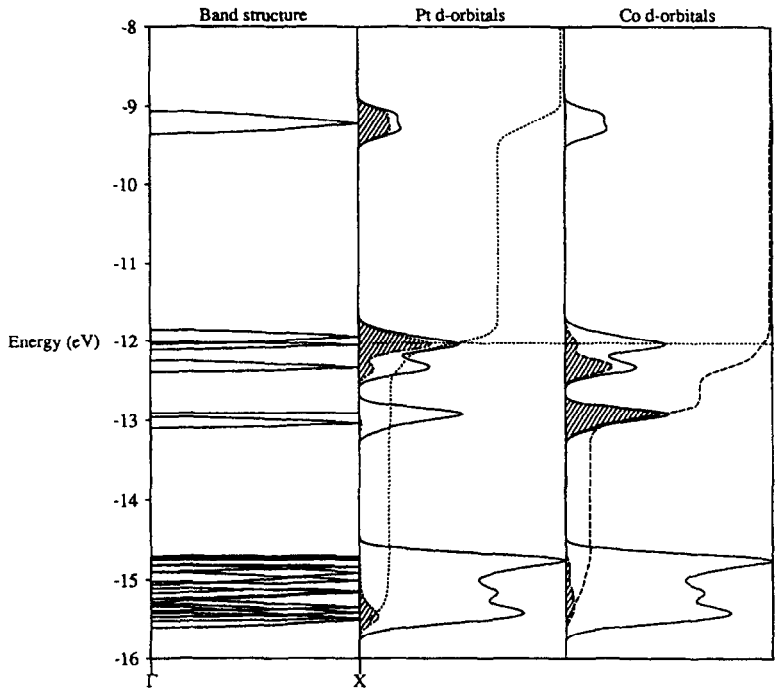

Fig. 3. From left to right: band structure for a $CoPtO_6^{6-}$ chain; total DOS (solid line), projection of Pt d-orbitals (lined), integration of the projection (dotted line); total DOS (solid line), projection of Co d-orbitals (lined), integration of the projection (broken line). The horizontal dotted line indicates the Fermi level.

sion a situation where randomly along the chain we will have weak antiferromagnetic interactions between nickel atoms separated by Pt(IV) as well as strong magnetic correlations between nickel atoms and adjacent Pt(II).

This magnetic behavior of Sr_3CoPtO_6 can be explained by the Random Spin Chain Paramagnetism model developed by Furusaki et al. [9], which predicts Curie-like paramagnetism for one-dimensional chains containing random ferro- and antiferromagnetic coupling constants. In such a system the magnetic ordering cannot be observed in the susceptibility data but can be detected by heat capacity measurements. Preliminary data indicate that the magnetic behavior of Sr_3CoPtO_6 is consistent with the theory of Furusaki et al.

The bonding interactions in the three isostructural oxides, Sr_3NiPtO_6, Sr_3CoPtO_6 and Sr_3NiIrO_6, are essentially identical based on the extended Hückel calculations. Their magnetic properties, however, differ significantly. While Sr_3NiPtO_6 only exhibits very weak antiferromagnetic interactions, Sr_3CoPtO_6 and Sr_3NiIrO_6 exhibit both ferro and antiferromagnetic correlations. It appears that diamagnetic metal centers, such as Pt(IV) (low spin d^6), do not participate in magnetic coupling via superexchange pathways, while paramagnetic metal centers, such as Ir(IV) (low spin d^5) and Pt(II) (low spin d^4), do promote magnetic coupling. Thus we observe long range magnetic order in both Sr_3CoPtO_6 and Sr_3NiIrO_6, where it appears that nearest neighbor electron coupling leads to ferromagnetic exchange interactions, while next nearest neighbor electron coupling in Sr_3NiPtO_6 leads to antiferromagnetic interactions. This observation is also consistent with antiferromagnetic coupling in Sr_3CuPtO_6 and Sr_3ZnIrO_6, and ferromagnetic order in Sr_3CuIrO_6, three structurally related chain compounds.

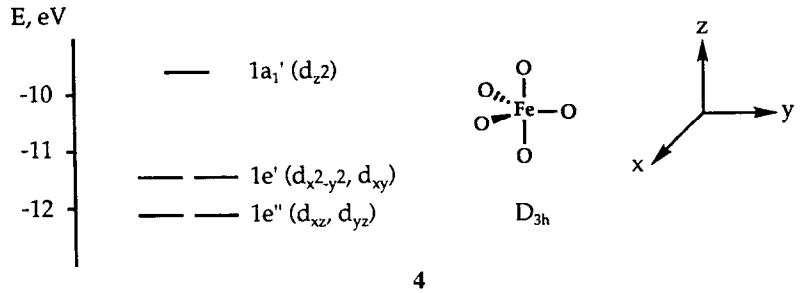

4

2.2. $InFeO_3$

$InFeO_3$, an oxide from the second group, consists of FeO_3 layers separated by In layers. As before, let us look first at the Fe d-orbitals in a model FeO_5^{7-} complex (assuming that iron here is formally Fe^{3+}). The energy levels, expected for a trigonal bipyramid, are shown in **4**.

When a two-dimensional sheet of FeO_3^{3-} stoichiometry is formed (in the *xy* plane), the 1e″ (d_{xz}, d_{yz}) and 1e′ (d_{xy}, $d_{x^2-y^2}$) levels generate fairly wide bands, while the $1a_1'$ (d_{z^2}) band is narrow (Fig. 8, see also Fig. 9 for the contributions of individual Fe d-orbitals). This is an indication of substantial intralayer Fe–O–Fe interaction. We suppose this interaction is responsible for the spin–spin superexchange giving rise to the antiferromagnetism found in $InMO_3$ oxides [2]. There is little direct Fe–Fe interaction, as measured by the OP, nor would much be expected, given the large Fe–Fe separation (3.327 Å). The calculated total Fe–Fe overlap population is

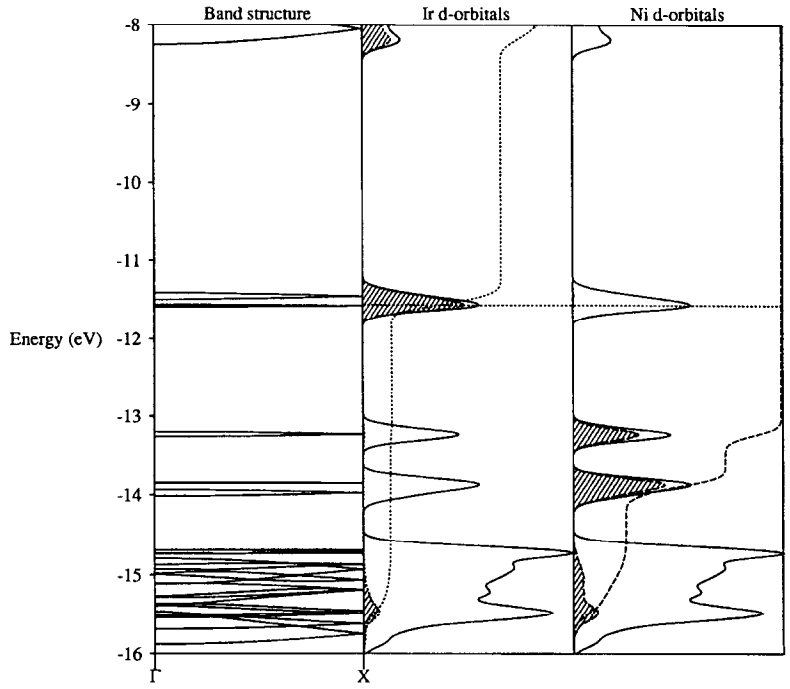

Fig. 4. From left to right: band structure for a $NiIrO_6^{6-}$ chain; total DOS (solid line), projection of Ir d-orbitals (lined), integration of the projection (dotted line); total DOS (solid line), projection of Ni d-orbitals (lined), integration of the projection (broken line). The horizontal dotted line indicates the Fermi level.

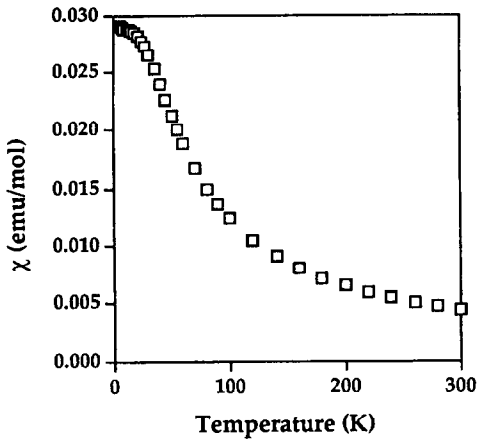

Fig. 5. Magnetic susceptibility of Sr_3NiPtO_6 at 5 kG.

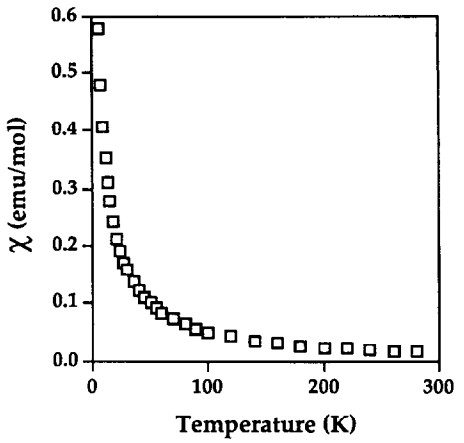

Fig. 7. Curie-like behavior of Sr_3CoPtO_6 corresponding to a moment of 5.96 μ_B.

0.0052. The total DOS and Fe d-orbital projections do not change much as we go from the two-dimensional sheet FeO_3^{3-} to a three-dimensional $InFeO_3$ crystal with In^{3+} ions included (also computed by us, but not presented here). This confirms the supposition that there is no significant interaction between FeO_3 layers. Calculations on $InMnO_3$ yield a band structure similar to that for $InFeO_3$; the Mn–Mn intralayer OP being 0.0012.

Magnetic measurements (Fig. 10) show that $InMnO_3$ orders in an antiferromagnetic-like fashion, $T_N = 15$ K. The magnetic behavior of $InFeO_3$ (not shown) is similar. The susceptibility vs. temperature plot displays a broad maximum at approximately 15 K at 0.5 kG. Changes in the inflection of the susceptibility curve are apparent at approximately 40 and 120 K. The application of an increasing magnetic field causes the susceptibility below the transition temperature to increase with decreasing temperature until the susceptibility plot appears featureless. Although $InMnO_3$ appears to be an antiferromagnet at 0.5 kG, all evidence of a magnetic transition at 15 K disappears at 40 kG (not shown).

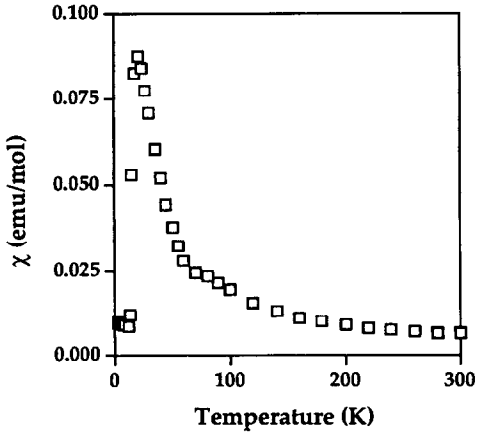

Fig. 6. Magnetic susceptibility of Sr_3NiIrO_6 at 40 kG.

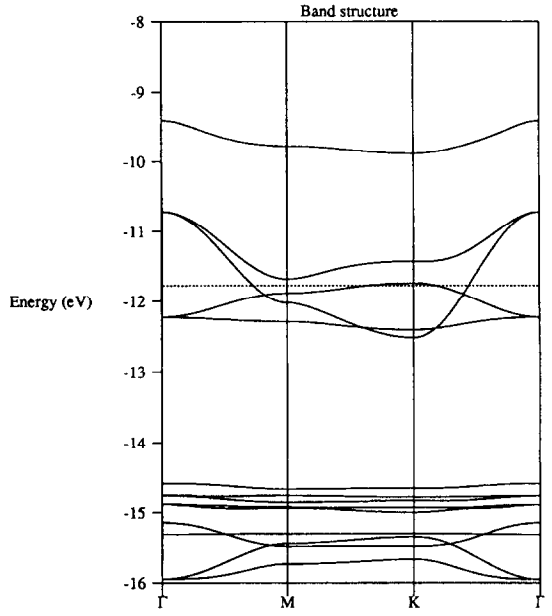

Fig. 8. Band structure for a two-dimensional FeO_3^{3-} sheet. The horizontal dotted line indicates the Fermi level.

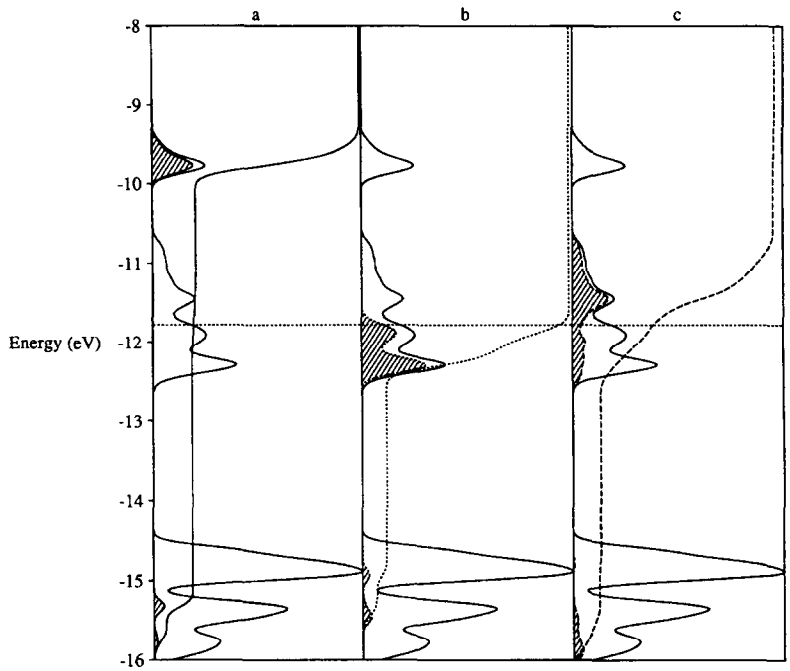

Fig. 9. Projections of Fe d_{z^2} (a), d_{xz} and d_{yz} (b), d_{xy} and $d_{x^2-y^2}$ (c). All projections are lined, the total DOS is also shown as well as integrations of the projections. The horizontal dotted line indicates the Fermi level.

Magnetic neutron data collected at temperatures ranging form 300 to 4.5 K indicate the existence of short range in-plane magnetic coupling [10]. The magnetic peaks were fit to a Warren line-shape, which manifests itself in powder diffraction data of samples that are two-dimensional in nature. A detailed analysis of the temperature dependence of the line shape indicates that intraplanar magnetic correlations in $InMnO_3$ are rigorously two-dimensional over the entire temperature range studied. The correlation length, L, increases from a room temperature value of 3.6(7) Å, which is essentially the nearest neighbor distance, to a maximum of 50 Å at lower temperatures. The magnitude of L changes slowly down to 120 K, when it rapidly increases, concomitantly with the appearance of weak short-range interplanar correlations.

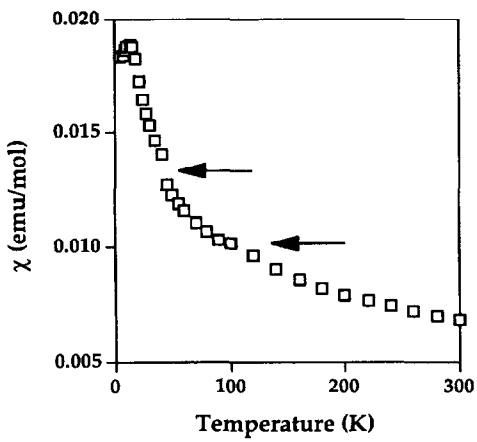

Fig. 10. Magnetic susceptibility versus temperature for $InMnO_3$ at 0.5 kG. A transition temperature is present at 15 K. Note inflections in the susceptibility curve at 40 and 120 K.

Although $InMnO_3$ never achieves true long range intra- or interplanar magnetic order, the predominant magnetic correlations are essentially confined to within the Mn–O layer. The band structure calculations indicate that there exist oxygen mediated bonding interactions between the manganese atoms located in the Mn–O layer but not, however, between the manganese atoms located in different Mn–O layers. This behavior is mimicked in the magnetic properties, where essentially all magnetic correlations are limited to within the Mn–O sheets. A large

part of that is, no doubt, due to the large distance between manganese atoms in different Mn–O sheets, which are separated by In–O octahedral layers that limit the extent of superexchange interactions.

There are two inherently limiting features of the extended Hückel method that should be pointed out here. The first one arises from the one-electron nature of the method: the energies of the orbitals as well as the energies of the bands do not depend on the number of electrons in the system. In other words, electron-electron interactions, such as those critical to the antiferromagnetic interactions considered above, are not taken into account explicitly. However, we can speculate about their magnitude based on the orbital interactions revealed by these very approximate calculations.

The second feature is especially important in the case of $InMO_3$ oxides. Mn^{3+} and Fe^{3+} ions are found experimentally to be in high spin configurations. In the band calculation the bands are just filled up, two electrons in each band, up to the Fermi level. Thus the population of Mn or Fe d-orbitals obtained in such a calculation differs from that expected for a high spin ion, which will certainly affect the values of COOP obtained. That is why relative energies and dispersions of d-bands need to be considered along with the overlap population analysis in order to evaluate the degree of M–M interaction.

Acknowledgement

Our work at Cornell was generously supported by the National Science Foundation through Research Grant CHE 94-08455. G.V. would also like to thank the Olin Foundation for financial support through a fellowship. The work at MIT was supported by the Massachusetts Institute of Technology, Center for Materials Science and Engineering under Grant DMR 9022933.

References

[1] T.N. Nguyen, D.M. Giaquinta and H.-C. zur Loye, Chem. Mater. 6 (1994) 1642;
H.-C. zur Loye, personal communications.
[2] D.M. Giaquinta, W.M. Davis, H.-C. zur Loye, Acta Crys. C 50 (1994) 5;
D.M. Giaquinta, H.-C. zur Loye, J. Am. Chem. Soc. 114 (1992) 10952; H.-C. zur Loye, personal communications.
[3] R.J. Hoffmann, J. Chem. Phys. 39 (1963) 1397. Tables of Parameters for Extended Hückel Calculations, collected by S. Alvarez, Universitat the Barcelona, 1993.
[4] C. Mealli and D.M. Prosperi, CACAO: Computer Aided Composition of Atomic Orbitals; available by anonymous FTP from: cacao.issecc.fi.cnr.it.
[5] N.N. Greenwood and A. Earnshaw, Chemistry of the elements (Pergamon Press, Oxford, 1989) p. 1345.
[6] C.J. Ballhausen, Introduction to ligand field theory (McGraw-Hill, London, 1962) p. 283.
[7] R. Hoffmann, Solids and surfaces: a chemist's view of bonding in extended structures (VCH; New York, 1988).
[8] T.N. Nguyen and H.-C. zur Loye, J. Solid State Chem. 117 (1995) 300.
[9] A. Furusaki, M. Sigrist, P.A. Lee, K. Tanaka and N. Nagaosa, Phys. Rev. Letters 73 (1994) 2622.
[10] J.E. Greedan, M. Bieringer, J.F. Britten, D.M. Giaquinta and H.-C. zur Loye, Synthesis, crystal structure and unusual magnetic properties of $InMnO_3$ J. Solid State Chem. 116 (1995) 118.